Utilization of Wavelet Packet Sensor De-noising for Accurate Positioning in Intelligent Road Services

Amr S. El-Wakeel[*†], Aboelmagd Noureldin[*†‡], Hossam S. Hassanein[*‡] and Nizar Zorba[†]

[*]Electrical and Computer Eng. Dept., Queen's University, Kingston, ON, Canada, K7L 3N6
[†]Electronics and Communications Eng. Dept., Arab Academy for Science & Technology, Cairo, Egypt
[†]Electrical and Computer Eng. Dept., Royal Military College of Canada, Kingston, ON, Canada, K7K 7B4
[‡]School of Computing, Queen's University, Kingston, ON, Canada, K7L 3N6
[†]Electrical Eng. Dept., Qatar University, Doha, Qatar
Email: {amr.elwakeel, nourelda}@queensu.ca, hosaam@cs.queensu.ca, nizarz@qu.edu.qa

Abstract—Recently, smart cities functionality and management have captured notable consideration. Owing to the rapid development in the information and communication technologies (ICT), various applications and services are highly engaged in the cities' operation. Specifically, intelligent road services as traffic management, driver behavior assessment and crowdsensing based road condition monitoring contribute towards better operability. To sustain decent performance of these applications, accurate and continuous positioning is an essential concern. Generally, Global Navigation Satellite System (GNSS) receivers are vulnerable to partial or complete outages due to multipath or signal blockage. Consequently, inertial navigation systems integrated with GNSS receivers are affected by inertial sensors noises and biases. In this paper, we apply wavelet packet de-nosing to eliminate noises of the Micro-Electro-Mechanical Systems (MEMS) grade inertial sensors. Afterwards, we integrate the de-noised reduced inertial sensor system (RISS) with GNSS receivers in real road experiment to assess the system performance. In addition, we show the significance of the proposed integration over the conventional one during multiple GNSS outages under various driving scenarios.

Keywords—Intelligent Road Services, GNSS, INS, Geo-referencing, Spectral Analysis, Wavelet Packet De-noising;

I. INTRODUCTION

The expeditious advancement of ICT is boosting smart cities services and functionalities. Correspondingly, Internet of Thing (IoT) world wide investment has been estimated to approach $772 billions in 2018 [1]. Consequently, broad IoT applications are confidently capable of serving smart cities dynamic operation, specifically in Intelligent Transportation Systems (ITS) and Road Information Services (RIS) components [2, 3]. In light of the vehicles motion sensors and smart devices, land vehicles are qualified to act as dynamic sensor hubs [2, 4]. Seeing figure 1, motion sensors (accelerometers, gyroscopes,..etc) and GNSS receivers can provide vital data to RIS cloud for analyzing and processing. This processed data can be used for providing information related to road surface conditions [2, 5], driver behavior [6, 7], trip planning [8] and traffic management [9].
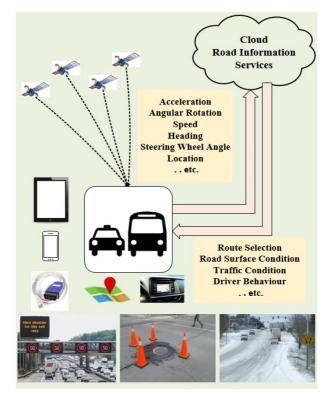
Figure 1. Cloud Road Information Services System Configuration.

Nevertheless, most if not all of these applications and services have a high demand of accurate and continuous location information. While the wide majority of the smart devices are equipped with GNSS receivers, they are considered the main key player in location determination for RIS. However, GNSS stand alone positioning solution may encounter high errors and uncertainties while providing geo-referencing [10]. On one hand, in down town and urban driving scenarios GNSS signals suffer from multipath or poor satellite geometry leading to partial or complete outages. On the other hand, complete outages

also occur while driving under bridges or in tunnels [10, 11]. To bypass these limitations, integrated positioning systems are adopted for providing continuous geo-referencing [10, 12].

Furthermore, integrating GNSS with Inertial Navigation Systems (INS) is the most popular forms of positioning integrations [13, 14]. Generally, inertial sensors mounted in land vehicles or embedded in ubiquitous smart devices are low MEMS grade. Therefore, during GNSS outages, INS geo-referencing solutions drift by virtue of inertial sensors noises and biases [13, 14]. For sensor noises, the low-frequency noises are named long term errors. On the contrary, high-frequency noises are called short term errors [15, 16].

In order to supress the inertial sensor noises consequences on the INS attainments, various filtering and spectral analysis techniques have been adopted in literature. In [17] a Daubechies wavelet-based de-noising technique was used to eliminate inertial sensor noise before integrating INS with GNSS. The proposed solution utilized soft thresholding for noise suppressing. Accordingly, the integrated system after de-noising was compared with low pass filtering (LPF) - based system integration. The results didn't show significant enhancement in terms of root mean square error, as the wavelet-based integrated system outperforms the LPF with approximately 20% only. Moreover, singular spectrum analysis was cascaded with independent component analysis to cut out accelerometers low-frequency noise [18]. However, the analysis neglected the effect of gyroscopes noises which have notable influence in INS. Also, it was assumed that the effects of the high-frequency noises were eliminated by Kalman Filter (KF), which is not always guaranteed. On the other hand, in [19] Fast Orthogonal Search (FOS) was adopted. It models the low-frequency band that contains the vehicle dynamics, to get rid of short and long-term errors of the inertial sensors. The main advantage of FOS is in the usage of a non-orthogonal candidate function that is capable of determining a frequency component between Fast Fourier Transform (FFT) bins. This technique can also averts the energy dissemination into another integer frequency component which is called spectral leakage [20]. The main limitation of the FOS algorithm in inertial sensor de-noising is that it divided the data into small windows to assume stationarity within each time window, which is not relevant in the case of high-frequency dynamics.

In this paper, we propose the adoption of Wavelet Packet De-nosing (WPD) for raw inertial sensors measurement in order to supress both low and high frequency noises. Consequently, in the proposed approach de-noising maintained both the low frequency vehicle dynamics and the high frequency that describe driver behaviour and road surface conditions. In addition, we integrate the de-noised RISS with GNSS utilizing closed loop Extended Kalman Filter (EKF). To show the improvement of the integrated positioning solution, we conduct real road trajectory and show the system results under 6 different GNSS outages including various driving scenarios.

II. System Structure

In this section, we present the system configuration used to integrate RISS/GNSS to provide a 3D positioning solution.
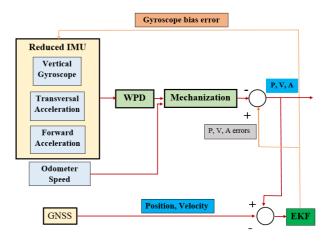

Figure 2. RISS/GNSS closed loop loosely coupled integrated positioning system. P, V and A are the position velocity and attitude, respectively.

In RISS, the gyroscope with its sensitive axis is aligned with the land vehicle vertical axis, the forward and transverse accelerometers, which together with a land vehicle odometer are all used to provide the INS solution [10, 21]. The main advantage of using the RISS is that the noises of the two discarded gyroscopes are avoided. As per figure 2. we use a closed loop 3D RISS loosely coupled integration, that is an efficient and low complexity when compared to the other integration methods [10].

A. Wavelet Packet De-noising

In Wavelet Analysis, the details in a signal are captured by a wavelet function, Ψ_t, and this operation is considered a high pass filtering. On the other hand, signal approximations are analyzed using a scaling function, ϕ_t, which is designed to smooth the input signal in a process equivalent to low pass filtering [22]. These two functions are usually orthonormal functions. The main drawback in utilizing wavelet analysis is some high-frequencies are suppressed while they may carry information about the driver behavior or a signature of a road anomaly [3, 23].

On the contrary, the wavelet packet analysis, as shown in Figure 3, applies an initial decomposition step that separates the signal into low-frequency approximation (A) and high frequency-details (D). Afterwards, both components are further decomposed for multiple levels, as the analysis aims to get fine resolution components of a signal [24].
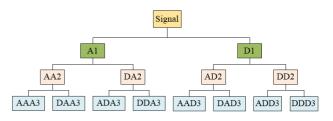

Figure 3. Wavelet Packet Analysis

1232

Initially, the analysis uses wavelet packet bases to break down the frequency axis into distributed splits with various sizes and these slots are translated in time to cover the whole time-frequency plane [22]. As any space, V_j, can be decomposed into sub-spaces of approximation, V_{j-1}, and details, W_{j-1}, where:

$$V_j = V_{j-1} + W_{j-1} \tag{1}$$

In the case of orthogonal bases, this is carried out by breaking the orthogonal basis of V_j into orthogonal bases for the approximation and details as $\{\phi_{j-1}(t - 2^{j-1}n)\}_{n \in \mathbb{Z}}$ and $\{\Psi_{j-1}(t - 2^{j-1}n)\}_{n \in \mathbb{Z}}$, respectively, this signal decomposition is specified by a pair of conjugate mirror filters $h[n]$ and $g[n] = (-1)^{1-n} h[n-1]$.

Due to sensor signals irregularities, nonlinear thresholding in wavelet bases is much promising than linear estimators. Regarding thresholds, we adopt the soft threshold mechanism of *Stein unbiased risk estimator* (SURE) provided in [22]. Reducing the thresholding risk could present through choosing a threshold less than $\sigma\sqrt{2log_e N}$, where σ is the noise standard deviation and N is the signal length. For the SURE thresholding [25, 26], the threshold value T, stands as:

$$T = \sqrt{2 \, log_e(Nlog_2(N)} \tag{2}$$

In our analysis, we utilize Daubechies wavelet family of order 8 and we apply 5 levels of signal decomposition. These selections assure the best performance while de-noising the inertial sensors in this work.

B. RISS/ GNSS Integration

Consequently, the de-noised sensor signals along with the odometer measurements are considered the inputs for the mechanization process. The navigation state vector of 3D RISS is given by $x = [\varphi, \lambda, h, v_e, v_n, v_u, r, p, A]^T$ as φ is the latitude, λ is longitude, h is altitude, v_e is the velocity towards east, v_n is the velocity towards north, v_u is the up velocity, r is the roll angle, p is the pitch angle, and A is the azimuth. Pitch angle is given by [10, 21]:

$$p = sin^{-1}\left(\frac{f_y - a_{od}}{g}\right) \tag{3}$$

Where f_y is the forward acceleration, a_{od} is the vehicle acceleration collected by the odometer, and g is the gravitational acceleration. The roll angle is computed as follows [10, 21]:

$$r = -\, sin^{-1}\left(\frac{f_x + v_{od}\omega_z}{g \cos p}\right) \tag{4}$$

The transversal acceleration is f_x, the vehicle speed extracted from the odometer measurement is v_{od}, the angular rotation around the vertical Z-axis is ω_z. Also, with the assumption of relatively low values of pitch and roll in 2D navigation, the azimuth angle is calculated as follows:

$$\dot{A} = -\left(\omega_z - \omega_e \sin \varphi - \frac{v_e \tan \varphi}{R_N + h}\right) \tag{5}$$

Where R_N is the normal radius of the earth curvature and h is altitude. All the linear acceleration and angular rotation are compensated for their biases and de-noised. Moreover, the three velocities can be transformed from forward velocity and calculated as follow:

$$v_e = v_{od} \, \sin A \, \cos p \tag{6}$$
$$v_n = v_{od} \, \cos A \, \cos p \tag{7}$$
$$v_u = v_{od} \, \sin p \tag{8}$$

R_M is the meridian radius of curvature, the latitude φ, the longitude λ, the altitude h, can be calculated as follow:

$$\dot{\varphi} = \frac{v_n}{(R_m + h)} \tag{9}$$

$$\dot{\lambda} = \frac{v_e}{(R_N + h) \cos \varphi} \tag{10}$$

$$\dot{h} = v_u \tag{11}$$

Gyroscope measurement error is the major source of error in 3D RISS the [10]. As it provides errors in horizontal velocity and positions which is not the case while using the accelerometers as their effects are small.

For the EKF, the discrete time domain is given by [10, 21]:

$$\delta x_{k+1} = \Phi_{k,k+1}\delta x_k + G_k w_k \Delta t \tag{12}$$

Given that the state transition matrix is $\Phi_{k,k+1}$, the error state vector is noted by δx_k, the noise parameter matrix is G_k, w_k is a Gaussian noise vector with a zero mean and Δt is the time interval. The system dynamic matrix F can be downsized to provide the state transition matrix Φ_k. The measurement model of the discrete KF is given by [13]:

The 3D RISS error state vector is provided by [21]:

$$\delta x = [\delta\varphi, \delta\lambda, \delta h, \delta v_e, \delta v_n, \delta v_u, \delta A, \delta a_{od}, \delta b_z]^T \tag{13}$$

where $\delta\varphi$ is latitude error, $\delta\lambda$ is longitude error, δh is altitude error, δv_e is east velocity error, δv_n is north velocity error, δv_u is upward velocity error, δA is azimuth error, δa_{od} is error in acceleration extracted from odometer measurements, and δb_z is gyroscope bias error. These equations are linearized to get the error model of the closed-loop EKF used for RISS/GNSS integration. This linearization process is performed by keeping only the first term of Taylor's series expansion. Accordingly, these linearized equations are used to build the F matrix, and the position of each term can be indicated by F_{mn}, where m is for the row, and n is for the column. These equations are given by [21]:

$$\delta\dot{\varphi} = \underset{F_{15}}{\underbrace{\frac{\delta v_n}{(R_M + h)}}} \tag{14}$$

$$\delta\dot{\lambda} = \underbrace{\frac{\delta v_e}{(R_N+h)\cos\varphi}}_{F_{24}} + \underbrace{\frac{v_e\,\tan\varphi}{(R_N+h)\cos\varphi}}_{F_{21}} \qquad (15)$$

$$\delta\dot{h} = \underbrace{\delta v_u}_{F_{36}} \qquad (16)$$

$$\delta\dot{v}_e = \underbrace{\sin A\cos p}_{F_{48}}\delta a_{od} + \underbrace{a_{od}\,\cos A\cos P}_{F_{47}} - \underbrace{\left(\omega_z - b_z - \omega_e\sin\varphi - \frac{v_e\tan\varphi}{R_N+h}\right)}_{F_{45}}\delta v_n + \underbrace{v_n}_{F_{45}}\delta b_z + \underbrace{v_n\left(\omega_e\cos\varphi + \frac{v_e\,sec^2\varphi}{R_N+h}\right)}_{F_{41}}\delta\varphi + \underbrace{\frac{v_n\tan\varphi}{R_N+h}}_{F_{44}}\delta v_e \qquad (17)$$

$$\delta\dot{v}_n = \underbrace{\cos A\cos p}_{F_{58}}\delta a_{od} + \underbrace{a_{od}\,\sin A\cos P}_{F_{57}}\,\delta A - \underbrace{\left(\omega_z - b_z - \omega_e\sin\varphi - \frac{2v_e\tan\varphi}{R_N+h}\right)}_{F_{54}}\delta v_e + \underbrace{v_e}_{F_{45}}\delta b_z + \underbrace{v_e\left(\omega_e\cos\varphi + \frac{v_e\,sec^2\varphi}{R_N+h}\right)}_{F_{51}}\delta\varphi \qquad (18)$$

$$\delta\dot{v}_u = \underbrace{\sin p}_{F_{68}}\delta a_{od} \qquad (19)$$

$$\delta\dot{A} = \underbrace{\delta b_z}_{F_{79}} + \underbrace{\left(\omega_e\cos\varphi + \frac{v_e\,sec^2\varphi}{R_N+h}\right)}_{F_{71}}\delta\varphi + \underbrace{\frac{\tan\varphi}{R_N+h}}_{F_{74}}\delta v_e \qquad (20)$$

The odometer and gyroscope errors are modeled as a Gauss-Markov process of the first order [25] and given by:

$$\delta\dot{a}_{od} = \underbrace{\beta_{od}}_{F_{88}}\,\delta a_{od} + \sqrt{2\beta_{od}\sigma_{od}{}^2}\,\omega(t) \qquad (21)$$

$$\delta\dot{b}_z = \underbrace{-\beta_z}_{F_{99}}\,\delta b_z + \sqrt{2\beta_z\sigma_z{}^2}\,\omega(t) \qquad (22)$$

Where $\boldsymbol{\beta}_{od}$ and $\boldsymbol{\sigma}_{od}$ are the Gauss-Markov process parameters for δa_{od}, while $\boldsymbol{\beta}_z$ and $\boldsymbol{\sigma}_z$ are for $\boldsymbol{\delta b}_z$. Thus, the full dynamic $\boldsymbol{F}$ matrix can be constructed given the terms denoted at each corresponding place, and the rest of terms are set to zero. Consequently, the measurement model for the loosely coupled integration of GNSS/INS gives the difference between the GNSS position/velocity and INS position/velocity as:

$$\delta z = H\,\delta x + v \qquad (23)$$

Where the measurements vector δz is given by:

$$\delta z = \begin{bmatrix} \varphi_{GNSS} - \varphi_{INS} \\ \lambda_{GNSS} - \lambda_{INS} \\ h_{GNSS} - h_{INS} \\ v_{e_{GNSS}} - v_{e_{INS}} \\ v_{n_{GNSS}} - v_{n_{INS}} \\ v_{u_{GNSS}} - v_{u_{INS}} \end{bmatrix} \qquad (24)$$

And the design matrix H is given as:

$$H = \begin{bmatrix} 1 & 0 & 0 & 0 & 0 & 0 & 0 & 0 & 0 \\ 0 & 1 & 0 & 0 & 0 & 0 & 0 & 0 & 0 \\ 0 & 0 & 1 & 0 & 0 & 0 & 0 & 0 & 0 \\ 0 & 0 & 0 & 1 & 0 & 0 & 0 & 0 & 0 \\ 0 & 0 & 0 & 0 & 1 & 0 & 0 & 0 & 0 \\ 0 & 0 & 0 & 0 & 0 & 1 & 0 & 0 & 0 \end{bmatrix} \qquad (25)$$

Where the term v is a Gaussian noise vector with zero mean with covariance matrix $R = \langle vv^T\rangle$.

III. RESULTS AND DISSCUSSION

In order to assess the significance of the WPD in RISS/GNSS integration. We held a road test experiment in Kingston, ON, Canada utilizing a land vehicle. The testbed shown in figure 4 was mounted in the land vehicle during the trajectory shown in figure 5. Regarding the equipment used, the MEMS-grade IMU provided by Crossbow (model IMU300CC-100) (Xbow) was utilized as the RISS component in the integration system and was logged at 100 Hz. The land vehicle forward speed was collected from the OBD interface using the CarChip device at a data rate of 1 Hz. To examine the performance of the proposed system, the reference solution was obtained by a NovAtel Span integrated solution. This solution is conducted by the integration of an OEM4 GPS receiver with fiber optic grade IMU-CPT logged at 100 Hz. Although the final navigation solution was provided at 1 Hz.

Figure 4. Testbed Utilized in Road Trajectory.

Figure 5. Road experiment in Kingston, ON, Canada, with 6 GNSS Outages.

1234

To show the significance of WPD, in figure 6 we compare the performance of the angular rotation measurement around the vertical axis of the MEMS grade Xbow before and after WPD with the reference high end IMU-CPT. Figure 6. Shows a time window of 35 seconds where the land vehicle had to complete successive turns. The figure illustrates the coincident performance of WPD measurements with the high end measurements provided by IMU-CPT.
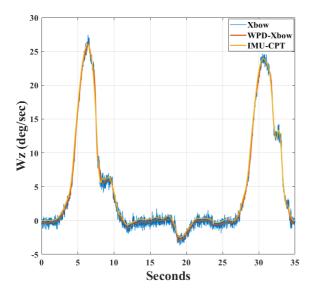

Figure 6. Angular rotation measurements around the vertical axis of Xbow, WPD-Xbow and IMU-CPT

TABLE 1. 2D RMS HORIZONTAL POSITION ERROR IN METERS DURING GNSS OUTAGES

OUTAGE No.	OUTAGE DURATION (SECONDS)	3D RISS/GNSS	WPD-3D RISS/GNSS
1	60	10.48	1.86
2	60	5.00	3.34
3	60	10.63	1.76
4	60	4.17	1.25
5	60	9.80	2.24
6	60	4.75	3.98
Average	60	7.47	**2.40**

TABLE 2. 2D MAXIMUM POSITION ERROR IN METERS DURING GNSS OUTAGES

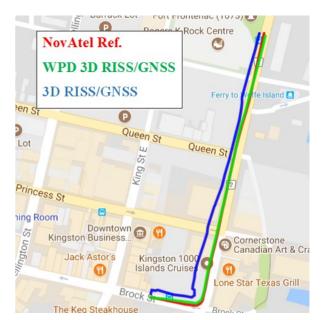| OUTAGE No.	OUTAGE DURATION (SECONDS)	3D RISS/GNSS	WPD-3D RISS/GNSS
1	60	20.28	5.35
2	60	9.23	5.59
3	60	17.68	6.89
4	60	12.53	3.26
5	60	8.08	7.73
6	60	6.48	6.07
Average	60	12.38	**5.81**

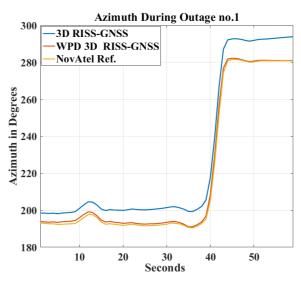Figure 7. Positioning solution during GNSS outage no.1

Figure 8. Azimuth of 3D RISS/GNSS, WPD 3D RISS/ GNSS and Novatel reference during GNSS outage no.1.

For further assessment, we examined and compared the performance of the WPD based RISS/GNSS integration system to the conventional RISS/GNSS during six simulated GNSS outages as shown in figure 5. All the outages were designed to be 60 seconds. While choosing the outages we considered multiple driving scenarios to include various dynamics such as straight driving, left and right turns, traffic lights stops, yields, stop signs and regular traffic frequent stops. Table 1 shows results of the 2D root mean square position error of the 3D RISS/GNSS and the WPD 3D RISS/ GNSS compared to the reference provided by NovAtel span unit. The results states that the WPD 3D RISS/GNSS provides average better positioning accuracy by approximately 68%. Regarding maximum 3D positioning errors, WPD 3D RISS/GNSS has enhanced the

1235

conventional 3D RISS/GNSS positioning errors by 53%. Moreover, figure 7 displays the continuous positioning solutions of 3D RISS/GNSS, WPD 3D RISS GNSS and NovAtel span reference solution during GNSS outage no.1. The outage includes two portions of straight driving separated by a right turn. The WPD 3D RISS/GNSS solution is within the road and almost coincide with reference solution while the 3D RISS/GNSS starts to drift since the early beginnings of the outage. Also, the azimuth results during the same outage presented in figure 8 supports the better performance of WPD 3D RISS/GNSS over the conventional one when compared to the reference azimuth.

IV. CONCLUSION

Intelligent road services receive high attention in smart cities operation. As they are highly related to residents safety and comfort. In order to sustain efficient performance of such services, accurate and continuous positioning are always required. Stand alone GNSS receivers suffer from partial or complete outages in downtown and urban canyons. While integrated INS/GNSS solutions are exposed to errors during GNSS outages as a result of inertial sensors noises. Leveraging WPD in RISS/GNSS, has improved the average 2D RMS positioning errors by 68 % while the average 2D maximum positioning errors by 53 % during typical GNSS outages in down town cores.

REFERENCES

[1] SmartCitiesWorld " IoT spending forecast to reach $772bn in 2018", 2017.

[2] J. Wahlström, I. Skog and P. Händel, "Smartphone-Based Vehicle Telematics: A Ten-Year Anniversary," *IEEE Trans. Intell. Transp. Syst.*, vol. 18, no. 10, pp. 2802-2825, Oct. 2017.

[3] A. S. El-Wakeel, J. Li, A. Noureldin, H. S. Hassanein and N. Zorba, "Towards a Practical Crowdsensing System for Road Surface Conditions Monitoring," *IEEE Internet Things J.*, vol. PP, no. 99, pp. 1-14, 2018.

[4] S. Abdelhamid, H. S. Hassanein and G. Takahara, "Vehicle as a resource (VaaR)," in *IEEE Network*, vol. 29, no. 1, pp. 12-17, Jan.-Feb. 2015.

[5] A. S. El-Wakeel, A. Osman, A. Noureldin and H. S. Hassanein, "Road Test Experiments and Statistical Analysis for Real-Time Monitoring of Road Surface Conditions," *GLOBECOM 2017 - 2017 IEEE Global Communications Conference*, pp. 1-6, Singapore, Dec., 2017.

[6] C. Miyajima and K. Takeda, "Driver-Behavior Modeling Using On-Road Driving Data: A new application for behavior signal processing," *IEEE Signal Process. Mag.*, vol. 33, no. 6, pp. 14-21, Nov. 2016.

[7] A. Abdelrahman, N. Abu-Ali and H. S. Hassanein, "Driver Behavior Classification in Crash and Near-Crash Events Using 100-CAR Naturalistic Data Set," *GLOBECOM 2017 - 2017 IEEE Global Communications Conference*, pp. 1-6, Singapore, Dec., 2017.

[8] X. Fan, J. Liu, Z. Wang, Y. Jiang and X. Liu, "Crowdsourced Road Navigation: Concept, Design, and Implementation," *IEEE Commun. Mag.*, vol. 55, no. 6, pp. 126-128, 2017.

[9] Z. Ning, F. Xia, N. Ullah, X. Kong and X. Hu, "Vehicular Social Networks: Enabling Smart Mobility," *IEEE Commun. Mag.*, vol. 55, no. 5, pp. 16-55, May 2017.

[10] A. Noureldin, T. B. Karamat, and J. Georgy, Fundamentals of Inertial Navigation, Satellite -based Positioning and their Integration. Springer - Verlag Berlin Heidelberg, 2013.

[11] S. Zhao, Y. Chen and J. A. Farrell, "High-Precision Vehicle Navigation in Urban Environments Using an MEM's IMU and Single-Frequency GPS Receiver," *IEEE Trans. on Intell. Transp. Syst.*, vol. 17, no. 10, pp. 2854-2867, Oct. 2016.

[12] J. Farell and M. Barth, The Global Positioning Systems and Inertial Navegation. McGraw-Hill, 1999.

[13] A. Noureldin, T. B. Karamat, M. D. Eberts, and A. El-Shafie, "Performance enhancement of MEMS-based INS/GPS integration for low cost navigation applications," *IEEE Trans. Veh. Technol.*, vol. 58, no. 3, pp. 1077–1096, 2009.

[14] J. Gao, K. Li and Y. Chen, "Study on Integration of FOG Single-Axis Rotational INS and Odometer for Land Vehicle," *IEEE SensJ.*, vol. 188, no. 2, pp. 752-763, Nov. 2017.

[15] N. El-Sheimy, S. Nassar and A. Noureldin, "Wavelet de-noising for IMU alignment," *IEEE Aerosp. Electron. Syst. Mag.*, vol. 19, no. 10, pp. 32-39, Oct. 2004.

[16] N. El-Sheimy, H. Hou and X. Niu, "Analysis and Modeling of Inertial Sensors Using Allan Variance," *IEEE Trans. Instrum. Meas*, vol. 57, no. 1, pp. 140-149, Jan. 2008.

[17] C.W. Kang, C.H. Kang, and C.G. Park, "Wavelet De-Noising Technique for Improvement of the Low Cost MEMS-GPS Integrated System". In *Proceedings of International Symposium on GPS/GNSS*, Taipei, Taiwan, 26–28 Oct. 2010.

[18] Z. W. Wu, M. L.Yao, H. G. Ma and W. M. Jia "De-noising MEMS Inertial Sensors for Lowcost Vehicular Attitude Estimation Based on Singular Spectrum Analysis and Independent Component Analysis", Electron. Lett., vol. 49, no. 14, pp. 892–893, Jul. 2013.

[19] A. Noureldin, J. Armstrong, A. El-Shafie, T. Karamat, D. McGaughy, M. Korenberg, A. Hussain "Accuracy Enhancement of Inertial Sensors Utilizing High Resolution Spectral Analysis," *Sensors*, vol. 12, no.9, pp. 11638-11660, 2012.

[20] K. H. Chon, "Accurate Identification of Periodic Oscillations Buried in White or Colored Noise using Fast Orthogonal Search," *IEEE Trans. Biomed. Eng.*, vol. 48, pp. 622-629, 2001.

[21] T. B. Karamat, M. M. Atia, and A. Noureldin, "An enhanced error model for EKF-based tightly-coupled integration of GPS and land vehicle's motion sensors," Sensors, vol. 15, no. 9, p. 24269, 2015.

[22] S. Mallat, A Wavelet Tour of Signal Processing: The Sparse Way, 3rd ed. New York: Academic Press, 2008.

[23] A. S. El-Wakeel, J. Li, M. T. Rahman, A. Noureldin and H. S. Hassanein, "Monitoring Road Surface Anomalies Towards Dynamic Road Mapping for Future Smart Cities," in *IEEE Global Conference on Signal and Information Processing (GlobalSIP)*, Montreal, CA, Nov. 2017

[24] L. Lau, "Wavelet packets based denoising method for measurement domain repeat-time multipath filtering in GPS static high-precision positioning applications", *GPS Solut.*, vol. 21, no. 2, pp 461–474, Apr. 2017.

[25] C. M. Stein, "Estimation of the mean of a multivariate normal distribution," *Ann. Statist.*, vol. 9, no. 6, pp. 1135–1151, 1981.

[26] Xiao-Ping Zhang and M. D. Desai, "Adaptive denoising based on SURE risk," *IEEE Sig. Proc. Lett.*, vol. 5, no. 10, pp. 265-267, Oct. 1998.
.